QUANTUM EFFICIENCY AND PHOTOVOLTAIC PROPERTIES OF A PHOTODIODE MADE OF POLY (3-4(-OCTYLPHENYL)-2, 2′-BITHIOPHENE) (PTOPT)

A thesis Presented to the
School of Graduate Studies
Addis Ababa University

In Partial Fulfillment
of the Requirements for the Degree
of Master of Science in Physics

By
Abay Gadisa

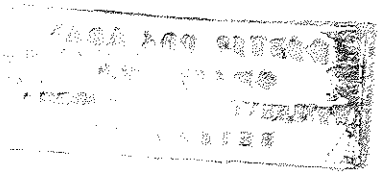

October 2000
Addis Ababa

ACKNOWLEDGEMENTS

I am indebted to my advisor, Dr. Bantikassegn Workalemahu, for excellent guidance, encouragement, and unlimited support during the time of the whole work. The friendly working environment he has created is quite appreciable and acknowledged.

I wish to express my gratitude to the Department of Physics, Addis Ababa University.

I would like to thank the International Center for Theoretical Physics (ICTP) for the financial support throughout my study.

A special thanks goes to the International Program in the Physical Sciences (IPPS) for providing us with most of the necessary laboratory equipment.

I would also like to express my gratitude to the Department of Chemistry, Addis Ababa University, for allowing me to use an optical set-up in their Electrochemical Research Laboratory.

Finally, I would like to thank my friends- Tesfaye Ayalew who introduced me to the laboratory work, Teshome Kormie, Etana Shibru, and Fekadu Mekonnen for their support and encouragement.

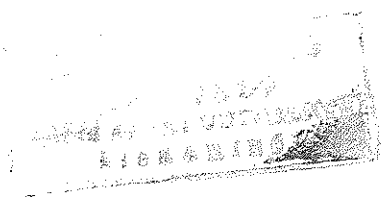

Abstract

In this thesis we investigated the photovoltaic properties of poly [3-(4-octylphenyl)-2, 2′-bithiophene] (PTOPT) in the form of Al/PTOPT/ITO sandwich structure. The peaks of the spectral response of the device were found to match with the absorption spectrum of PTOPT for illumination from both the Al and ITO sides. However, the IPCE% obtained when the device was illuminated from the Al side is found to be lower than for illumination from the ITO side. The experimentally collected data on absorption and action spectrum are explained based on the theoretical model proposed by Gosh and Feng. The photovoltaic parameters were determined from the I-V curve recorded by illuminating the photodiode through the Al side with monochromatic light (500 nm) of intensity 7.4 $\mu W/cm^2$. No correction was done for reflection from the surface of the Al electrode. A power conversion efficiency of 0.7% and a fill factor of 0.25 were also obtained. The small value of the efficiency is due to the low mobility of the charge carriers of the photodiode. Moreover, the short circuit photocurrent of the device was found to vary with the incident light intensity. The observed variation of the photocurrent with the incident light irradiation (linear at low light intensities and non-linear at higher light intensities) will be explained using a simple kinetic model.

Contents Page

List of figures Page

List of Tables Page

1. Introduction

Solar energy is an inexhaustible and most important source of renewable energy. The annual solar energy incident on Earth (5% UV, 43% Visible, 52% IR) [1] exceeds the world's yearly energy consumption by several thousands. It is only about 0.03% of the solar energy that is stored as chemical energy by the photosynthetic process of green plants that provide all our food and has generated the fossil fuels.

By using solar energy as our future source of energy we can avoid the severe problems that arise due to exhaustibility of the irreplaceable reserve of fossil fuel and the rapid degradation of the global environment. As a result extensive research has been undertaken to convert solar energy directly into electrical energy using photovoltaic cells. Today, this method has become one of the most promising fields of research on renewable energy.

Inorganic semiconductor materials like silicon and germanium form the basis for the vast majority of research and development work in the area of photovoltaic devices. In 1954 the solar energy conversion efficiency of a single-crystal silicon cell was reported to be 6% [2]. Currently, not only the physics of the inorganic semiconductors is well understood, but also conversion efficiency as high as 25% has been attained in laboratory condition [3,4]. Eventhough these inorganic materials have been used in various optoelectronic devices, they are not yet utilized at a larger scale due to high manufacturing costs.

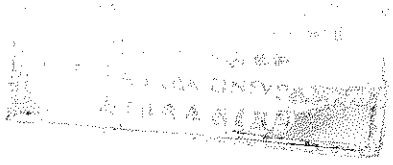

In the past few years, several attempts have been made to use organic semiconductors as active components in electronic and optical devices. Particularly, merocyanines and pathalocyanines [1,5] are the most studied organic compounds because of their good chemical stability and great optical absorption in the visible region of the solar spectrum. In addition, they can be readily deposited as a thin film on various substrates by vacuum evaporation. Photovoltaic cells have also been fabricated using conjugated polymer films such as poly (N-vinylcarbazole)- trinitrofluorene [6], polyacetylene [7], various derivatives of polythiophene [8,9], and poly(p-phenylenevinylene) and its derivatives [8,10,11].

There are some barriers to the successful utilization of polymeric photodiodes such as their extremely complex structures and poor conversion efficiencies. Efficiencies close to 1% have been reported for undoped single layer organic photovoltaic devices [5,6, 12-14] and as close as 2% for interpenetrable network polymeric devices [9,15] under a simulated solar spectrum.

On the other hand, several features of organic semiconductors make them attractive candidates for use in photovoltaic devices. They are inexpensive and readily available. Unlike the inorganic semiconductors, polymeric semiconductor devices are easy to fabricate. In addition, they can be used in thin-film forms that reduce the material cost.

The objective of this experimental research work is to investigate the photoelectric properties of poly [3-(4-octylphenyl)-2, 2′-bithiophene] (PTOPT) in the form of Al/PTOPT/ITO sandwich structure where aluminum (Al) and indium tin oxide (ITO) coated on a glass, commercially available, serve as contact electrodes. PTOPT is an organic polymer that was studied for its electrical properties and found out to give a very high rectification ratio [16]. This is indicative of its being a candidate for characterization of photovoltaic properties as well as yielding high quantum efficiency. PTOPT is one of the most stable polymers towards light synthesized as a derivative of polythiophene. In this thesis, the I-V characteristics of the device in the dark and under illumination were measured. The photoaction spectra of the device were also measured and analyzed. Various photovoltaic parameters such as short-circuit photocurrent density (J_{sc}), open-circuit voltage (V_{oc}), fill factor (FF), and power conversion efficiency (η) were calculated from the I-V characteristic under illumination of the device through the Al electrode and reported.

2. Basic Properties of Electrically Conducting Polymers

Polymers are organic molecules synthesized by bonding many small repeating units known as monomers. They are large molecules, often known as macromolecules, with molecular weight measured in hundreds of thousands of molar weight. Most polymers are elastic, frictional resistant, tough, and insulators.

The existence of conducting polymers was realized in 1970's when oxidized polyacetylene with metallic appearance [17] was accidentally synthesized. This was further confirmed when the electrical conductivity of polyacetylene was investigated to vary with 'doping' level [18,19] (an oxidation or reduction process). Using samples of doped *trans*-polyacetylene, conductivities almost as high as 10^5 S/cm were obtained [20], which is comparable to that of copper.

Apart from polyacetylene, the electrical conductivity of several conjugated polymers has been extensively studied. Particularly, the electrical conductivity of conjugated polymers, polymers with alternating single and double bonds, varies over the full range from insulator through semiconductor to metallic by p-doping (oxidation) or n-doping (reduction). These polymers are candidates to become substitutes of familiar inorganic semiconductors in many applications because of their high absorption in the visible range of the solar spectrum, and low cost of fabrication. The chemical structures of some conjugated conducting polymers are shown in Fig. 2.1.

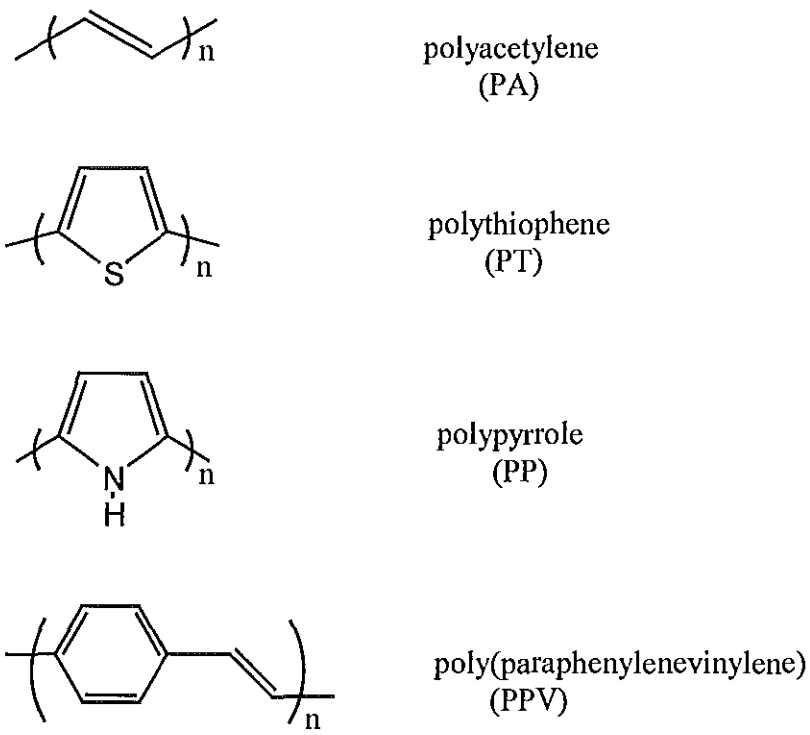

Fig. 2.1 Chemical structures of some conjugated polymers.

Extensive research has been carried out on the use of conducting polymers as active materials in opto-electronic devices. Undoped or doped conjugated polymers, such as polyaniline [21], and polythiophene and its derivatives [22,23], have shown semiconducting behavior that may be utilized in electrical device applications. In general, use of organic thin films in the electrical and optical devices is a subject of current interest of many researchers [24-26].

2.1 Electrical Properties

The ground state electronic configuration of atomic carbon is $1s^2 2s^2 2p_x^1 2p_y^1 2p_z^0$. One of the 2s electrons jumps to the empty p-orbital when the atomic carbon is in its excited state, thereby changing the atomic orbital

configuration to $1s^2 2s^1 2p_x^1 2p_y^1 2p_z^1$. Accordingly, the molecular orbitals of carbon are described as hybrids formed from the 2s, $2p_x$, $2p_y$, and $2p_z$ atomic orbitals.

Polyacetylene, $(CH)_x$, is the most studied polymer because of its regular, and linear structure. Better understanding of physical and electrical properties of other conjugated polymers is based on the theory of that of polyacetylene.

The carbon atoms in ethene molecule, the monomer of polyacetylene, are sp^2 hybridized and are connected to each other and to hydrogen atoms by σ-bonds. The carbon p_z- orbitals interact with each other forming two orbitals known as bonding (π) and antibonding (π^*) molecular orbitals (MOs). Since each of the p_z-orbital contributes one electron, the bonding (π) orbital is occupied by two electrons in the ground state.

There is a discrete optical transition between the two molecular orbitals, the highest occupied molecular orbital (HOMO) and the lowest unoccupied molecular orbital (LUMO).

In a similar way, the simplest conjugated hydrocarbon 1,3-butadiene has two bonding (π) orbitals and two antibonding (π^*) orbitals. Each of the bonding orbitals is occupied by electron pairs while the antibonding (π^*) ones are empty. The next simple conjugated hydrocarbon is 1,3,5-hexatriene with three fully occupied bonding (π) orbitals and three empty antibondig orbitals (π^*). As more and more monomer units (ethene) are added, longer and longer conjugated molecules will be created which finally results into the macromolecule polyacetylene which contains very many number of bonding (π) and antibonding

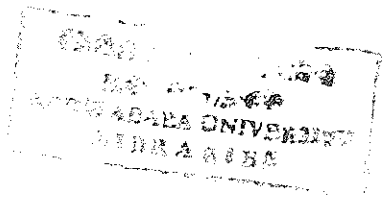

(π^*) MOs. The extremely large number of bonding (π) and antibonding (π^*) MOs are closely spaced and hence form an approximately continuous energy band levels. The band of fully occupied bonding (π) molecular orbitals (HOMO) is known as valance band (VB) and the band of vacant antibonding (π^*) molecular orbitals (LUMO) is known as conduction band (CB), and the two bands are separated by the energy gap or forbidden gap.

Materials are classified as metal, semiconductor, or insulator depending on their energy band structures. Metals are characterized by partially filled energy bands while semiconductors and insulators are characterized by their completely filled valence band and completely empty conduction band. Semiconductors differ from insulators by their relatively smaller energy gap. Pure conjugated polymers are insulators or at most semiconductors.

Polymers are quasi one-dimensional chains and hence the analysis of the physics of one-dimensional metals is important to understand the transition from pure metallic state to semiconducting state [27].

Trans-polyacetylene has two degenerate ground states that are assumed to be with no misfits or domain walls as shown in Fig. 2.2.

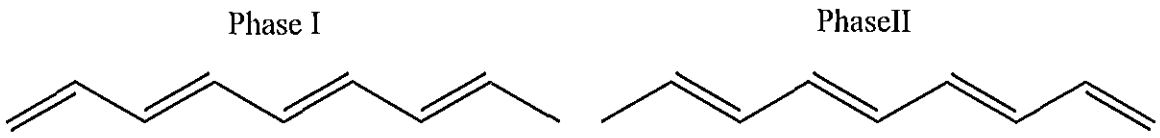

Fig. 2.2 Ground state trans-polyacetylene

There is a chance of getting the two degenerate states of *trans*-polyacetylene on the same chain, separated by a misfit or domain wall. These domain walls, shown in Fig. 2.3, which may be formed when the polymer is being synthesized or doped are conjugational defects and known as solitons.

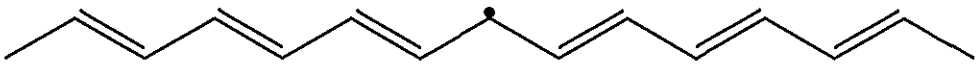

Fig. 2.3 A domain wall (soliton) separating the two phases of *trans*-polyacetylene.

The cause of gap formation is the uninterrupted double and single bond alternation. But the bond alternation is interrupted at the soliton site. Thus, the atomic orbitals at the misfit are neither bonding (π) nor antibonding (π^*) state. As a result, the state of the unpaired electron resides in a non-bonding orbital, which is created at the middle of the forbidden gap. As shown in Fig. 2.4, the soliton is positively charged with spin zero when the electron is removed and negatively charged with spin zero when an electron is added. However, neutral solitons have spin ½.

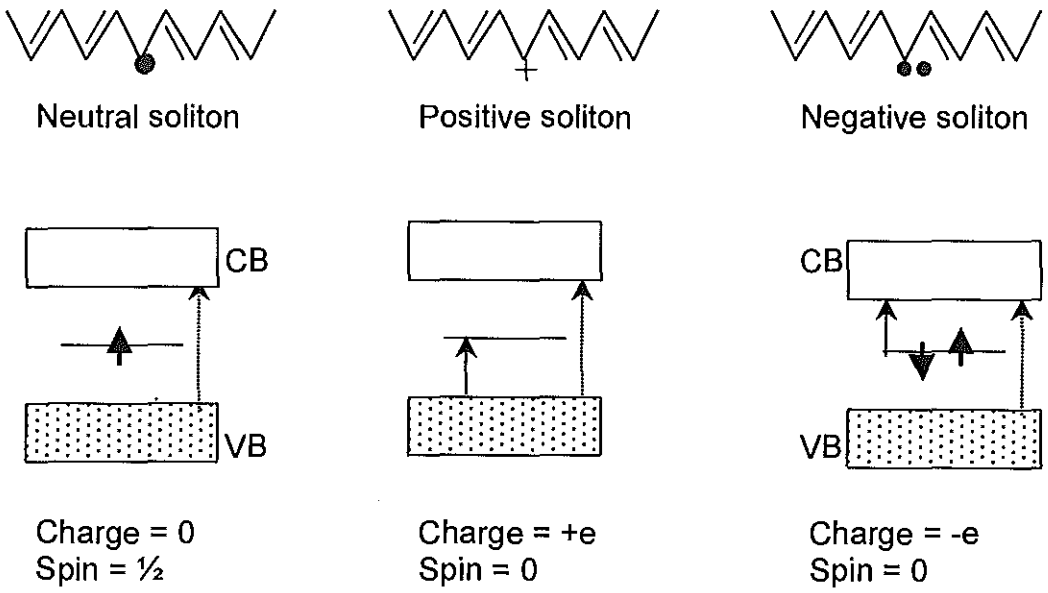

Fig. 2.4 Solitons and their corresponding energy band diagrams with the allowed interband (dashed arrow) and subgap (thin solid arrow) transitions. Short arrows represent electron spins.

Several conjugated polymers, including *cis*-polyacetylene, have non-degenerate ground states known as aromatic and quinoidal .

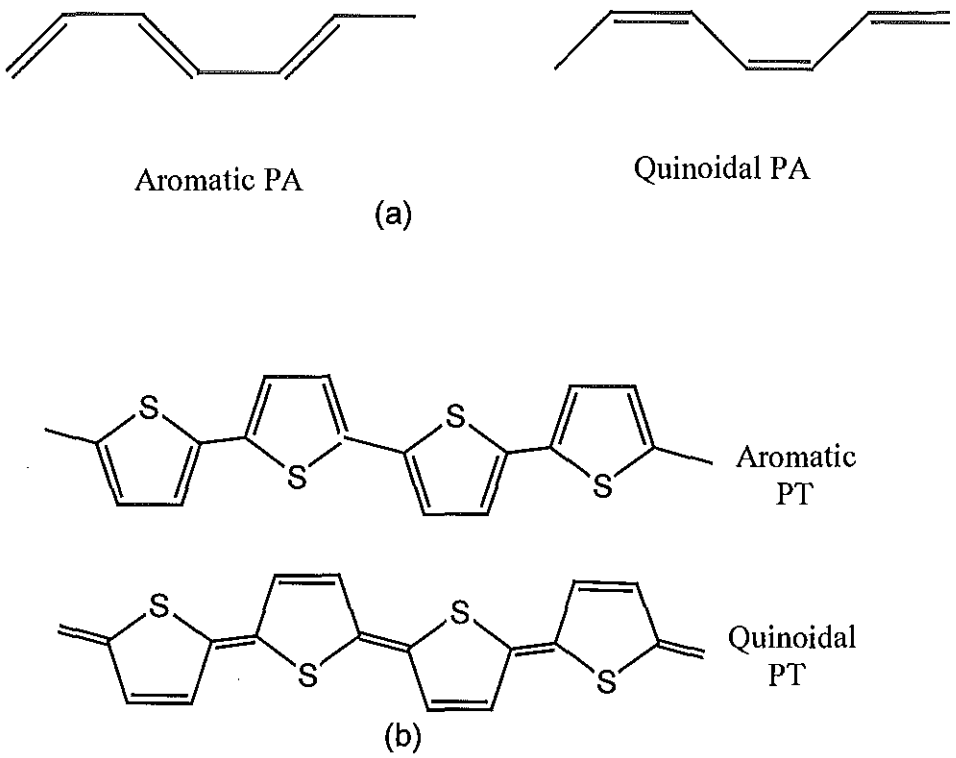

Fig. 2.5 The aromatic and quinoidal forms of (a) *cis*-polyaceteylene and (b) polythiophene.

The energy of the aromatic form is lower than that of the quinoidal form. Hence the left and the right sides of the misfit in polythiophene, shown in Fig. 2.6, have different energies. This energy difference makes the misfit or soliton energetically unstable. Consequently, the soliton moves in the direction shown in Fig. 2.6 and changes the high-energy quinoidal rings into low energy aromatic rings. These defects will be stable if and only if bound-double defects, known as polarons, are formed.

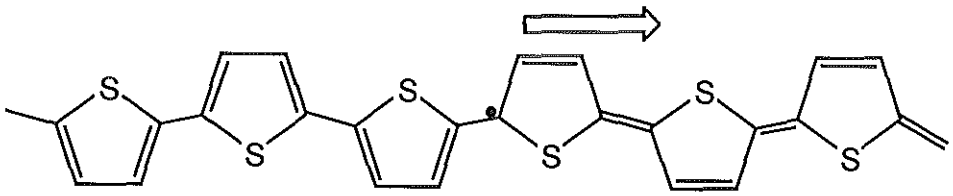

Aromatic Quinaidal

Fig. 2.6 The direction of motion of soliton in polythiophene.

In general, if an electron is removed from the polymer, a polaron is generated accompanied by the change of quinoidal state into aromatic state. Removal of one additional electron from the same polymer leads to the formation of a doubly charged defect known as bipolaron. These states are shown in Fig. 2.8 (a), and (b), respectively. Hence a polaron is formed from two solitons in a single chain where one of the solitons should be a neutral soliton, and a bipolaron is formed from two positively charged solitons or two negatively charged solitons.

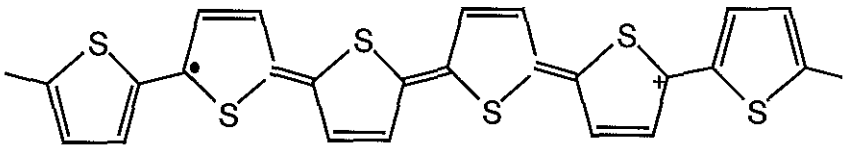

(a)

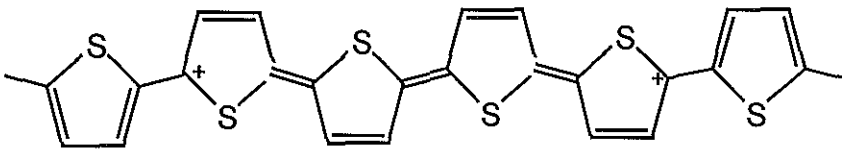

(b)

Fig. 2.7 The two states of polythoiophene (a) hole polaron, and (b) hole bipolaron.

Unlike the single midgap state of solitons, the existence of polaron or bipolaron results into the creation of two midgap states.

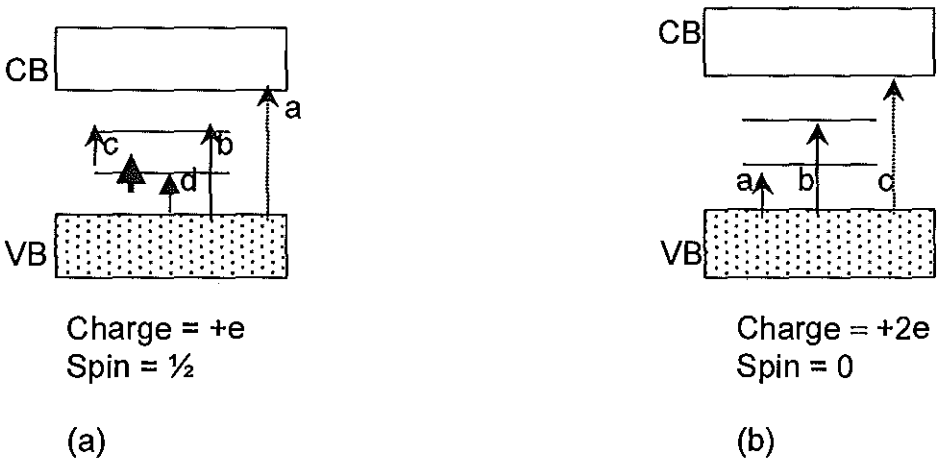

Fig. 2.8 Energy band diagram for (a) a hole polaron and (b) a hole bipolaron with their possible optical transitions.

As depicted in Fig. 2.8, a hole polaron has four possible transitions while a hole bipolaron is limited to only three optical transitions because the two gap states are empty and hence transition from the lower state to the upper state is not observable. The existence of the two midgap states with their possible optical transitions is confirmed by optical absorption spectroscopy. The optical absorption spectra of PTOPT is depicted in Fig. 2.9

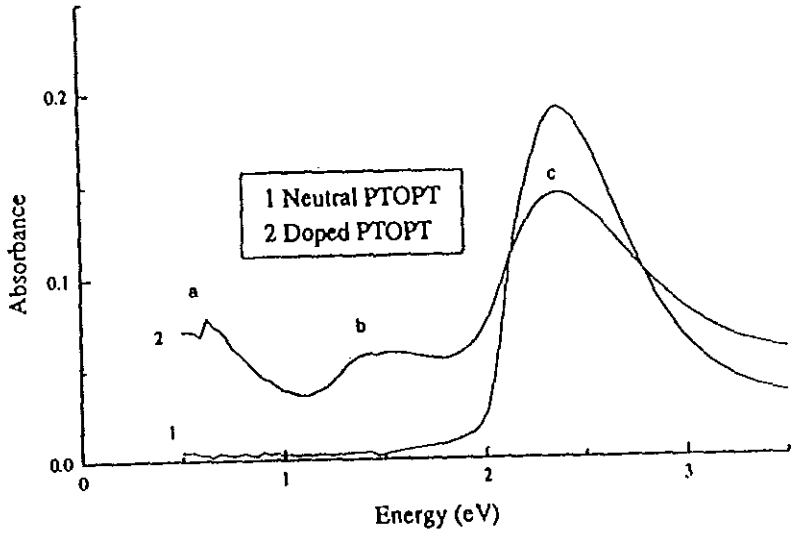

Fig. 2.9 Optical absorption spectrum of PTOPT neutral and lightly doped with $NOPF_6$. Labels a, b, and c are absorption peaks corresponding to transitions shown in Fig. 2.8 (b) [16].

2.2. Charge Transport Mechanisms and Electrical Conductivity

The conductivity of undoped organic semiconductors is very low. This low conductivity of organic semiconductors may lead to the conclusion that the free carrier concentration is much lower than the impurity concentration. This is because the impurity sites trap most of the free carriers resulting into recombination of electron-hole pairs. On the other hand, doping of conjugated polymers introduces more charge carriers on the polymer chain, and hence enhances the conductivity by several orders of magnitude.

Conductivity highly depends on temperature of a material. For pure metals conductivity increases with decreasing temperature since cooling the metal

reduces the lattice vibrations which act as barriers to charge carriers. On the contrary, cooling an organic semiconductor freezes out both the lattice vibrations and the charge carriers. Consequently, the conductivity of organic semiconductors decreases on decreasing temperature.

As a result of complex structural and morphological forms of conjugated polymers, a single model may not be applicable to different polymers to understand the charge transport mechanisms in their conductivity regions.

The electronic states responsible for charge transport in undoped conjugated polymers are localized and have low mobility. This phenomena is true also in amorphous semiconductors where conduction by free charge carriers is not possible as the free electrons become localized and can only move by hopping (phonon-assisted quantum mechanical tunneling) between localized states located in the forbidden gap. Accordingly, the Mott's variable range hopping (VRH) theory [28,29], which was proposed to explain the conductivity of amorphous semiconductors, is applied for undoped or lightly doped conjugated polymers in order to understand the charge transport mechanism between their localized solitonic, polaronic, and bipolaronic states. VRH is a thermally agitated process in which the conduction mechanism is dominated by electron hopping near the Fermi level. According to the VRH model, the temperature dependence of conductivity is given by

$$\sigma = \sigma_0 \exp[-\left(\frac{T_0}{T}\right)^{\gamma}] \qquad (2.1)$$

where σ_0 and T_0 are fitting parameters which are generally experimentally determined, and γ depends on the dimensionality d of the hopping process and is given by

$$\gamma = \frac{1}{1+d} \qquad (2.2)$$

In three dimensional hopping d =3, and γ =4 and hence

$$\sigma = \sigma_0 \exp[-\left(\frac{T_0}{T}\right)^{1/4}] \qquad (2.3)$$

Mott's model has been shown to be appropriate for polyacetylene [30], poly(3-alkylthiophene) [31] and polypyrrole [32].

For highly doped conducting polymers, the VRH model disagrees with experimental results. The Sheng model [33,34], which assumes that conduction takes place between highly conductive islands separated by potential barrier, is found to be appropriate to explain the charge transport mechanism in highly doped conducting polymers. In this model the process of charge transfer takes

place due to the tunneling enhanced by thermal fluctuations at higher temperature through the barriers. The temperature dependence of conductivity, according to the Sheng's model, is given by

$$\sigma = \sigma_0 \exp\left(-\frac{T_0}{T_1 + T}\right) \tag{2.4}$$

where σ_0, T_0 and T_1 are constants to be determined by the geometry of the barrier and the size of the conducting islands. From eqn. (2.4), two limiting cases can be derived:

(a) for $T << T_1$, eqn. (2.4) leads to constant conductivity of the polymer given by

$$\sigma = \sigma_0 \exp\left(\frac{-T_0}{T_1}\right) \tag{2.5}$$

(b) for $T >> T_1$,

$$\sigma = \sigma_0 \exp\left(\frac{-T_0}{T}\right) \tag{2.6}$$

which is an expression for a thermally activated system.

3. Electrical and Photoelectrical Properties of Organic Photodiodes

The electrical properties of a metal/semiconductor contact is determined by the work functions of the metal and the semiconductor, where work function is the difference in energy between the Fermi level and the vacuum level [35]. Conducting polymer/metal contact is formed when the polymer is sandwiched between low work function metals such as aluminum or indium, and high work function metals such as gold or silver. Such a contact may be either ohmic or non-ohmic depending on the work functions of the polymer and the metal. The ohmic interface is non-rectifying whereas the non-ohmic interface may form a rectifying contact usually known as Schottky barrier.

Both ohmic and rectifying contacts play key roles in various semiconductor device applications. One of the uses of ohmic contact is to reduce resistance losses for almost all kinds of devices made of semiconductors [36]. Rectifying contacts, on the other hand, form critical parts in photovoltaic cells [6,7,37], photodetectors [36,37], transistors [38,39], and many other semiconductor devices.

The physics of inorganic semiconductor/metal contact is similar to that of polymer/metal contacts. If a semiconductor of a given work function is brought into contact with a metal having a different work function, charges will flow across the

interface until a thermal equilibrium is attained by equalizing the Fermi levels on both sides of the structure.

When an n-type semiconductor of work function ϕ_n, is in contact with a metal of higher work function ϕ_m, electrons in the conduction band of the semiconductor diffuse to the metal thereby creating a region depleted of majority carriers near the interface as shown in Fig. 3.1(b).

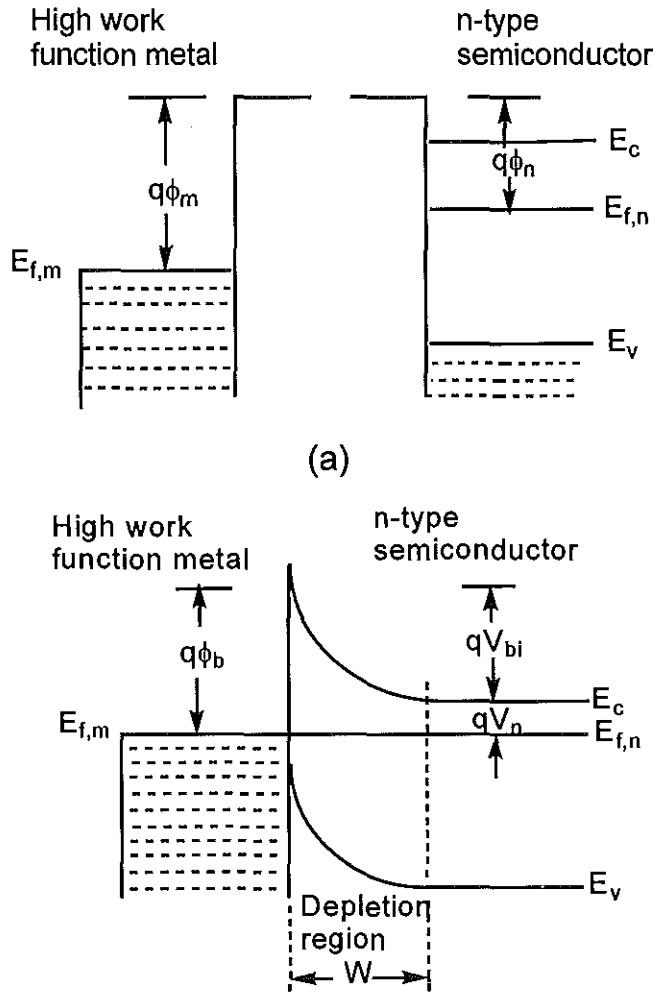

Fig. 3.1 Energy band diagram of a metal and n-type semiconductor (a) before contact, and (b) after contact at thermal equilibrium for $\phi_m > \phi_n$.

As can be seen from Fig. 3.1 (b), the depletion of charges results into bending of the conduction energy level (E_c) and the valence energy level (E_v) near the interface. These energy levels remain constant relative to the Fermi energy level (E_f) in the bulk of the semiconductor. Such a contact may manifest a rectifying character [35,36,40].

The physics of metal/semiconductor contacts can be explained using the important parameters shown in Fig. 3.1 (b), where W is the width of the depletion layer at thermal equilibrium. The parameter ϕ_b is the barrier height seen by electrons in the metal trying to diffuse into the semiconductor. It is given by

$$\phi_b = V_n + V_{bi} \tag{3.1}$$

where V_n is the difference between E_c and $E_{f,n}$ in the bulk of the semiconductor, and V_{bi} is the built-in potential. The potential barrier encountered by the electrons that diffuse from the semiconductor conduction band to the metal is

$$V_{bi} = \phi_m - \phi_n \tag{3.2}$$

and the potential barrier against the flow of electrons from the metal to the semiconductor is ϕ_b.

When $\phi_m < \phi_n$, electrons diffuse into the n-type semiconductor creating high density of majority carriers (electrons) in the semiconductor conduction band.

Hence, near the interface a very thin negatively charged layer is formed and the depletion layer becomes thin. Because charge carriers can easily tunnel through this thin layer, there will be a free current flow between the metal and the semiconductor in both directions. Such a contact is ohmic [35,36,40].

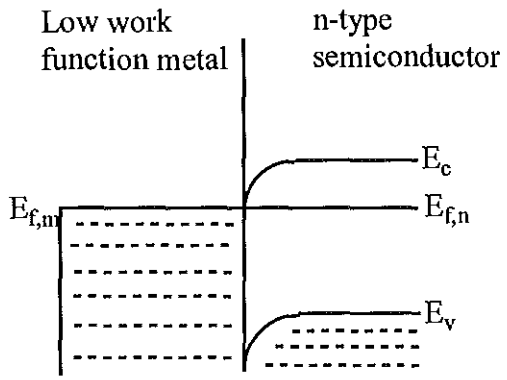

Fig. 3.2 Energy band diagram of a metal/n-type semiconductor contact at thermal equilibrium for $\phi_m < \phi_n$ (ohmic contact).

Similar analysis leads to a conclusion that an ohmic contact is formed when a p-type semiconductor of work function ϕ_p is brought into contact with a metal of higher work function ϕ_m. The contact is Schottky junction if $\phi_m < \phi_p$. The energy band diagram of both cases are depicted in Fig. 3.3.

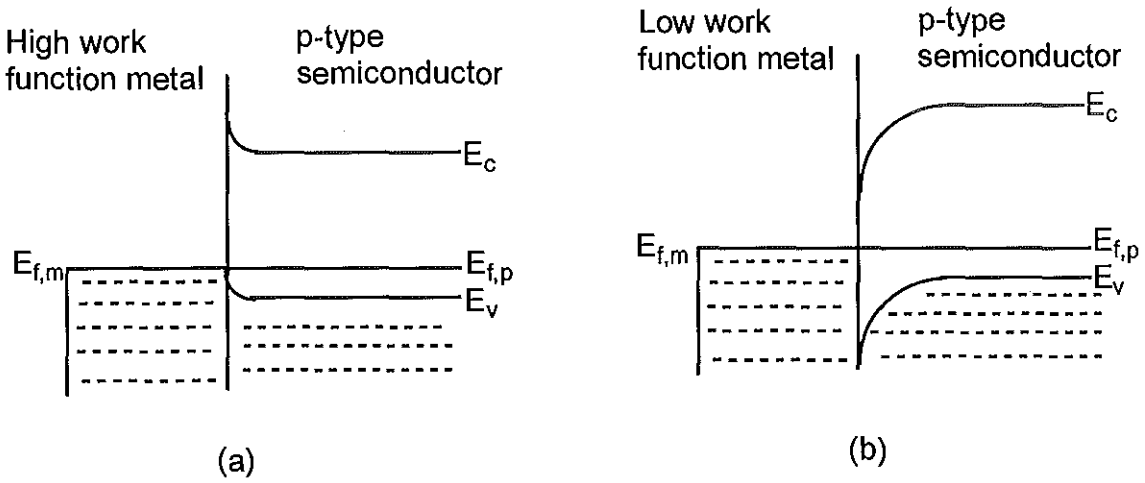

Fig. 3.3 Energy band diagram of metal/p-type semiconductor at thermal equilibrium (a) for $\phi_m > \phi_p$, and (b) for $\phi_m < \phi_p$.

3.1 Current-Voltage Characteristics

Majority carriers dominate the current transport in a metal/semiconductor junction. An externally applied field influences the charge carrier transport in Schottky barrier devices. When a forward bias voltage is applied across the junction, the effect of the internal barrier field reduces, which results into an increase in the number of carriers that cross the interface. On the contrary, applying a reverse bias voltage increases the internal barrier field which intern reduces the number of carriers that flow across the interface.

In general, the current-voltage characteristics of a Schottky diode in the dark is described by the thermionic emission theory as

$$J_d = J_s \left[\exp\left(\frac{qV}{nkT}\right) - 1\right] \qquad (3.3)$$

where J_d is the net dark current density, J_s is the reverse saturation current density, q is the electron charge, V is the forward bias voltage, n is the diode quality factor, k is the Boltzmann's constant, and T is the absolute temperature.

The reverse saturation current, J_s, is an important parameter that determines whether the junction is an ohmic, rectifying, or the mixture of both. It is given by

$$J_s = \mathrm{A}^{**}\,\mathrm{T}^2 \exp\left(-\frac{\mathrm{q}\phi_b}{\mathrm{kT}}\right) \tag{3.4}$$

where A^{**} is the modified Richardson constant, and ϕ_b is the barrier height. The modified Richardson constant, A^{**}, for organic semiconductor diodes is assumed to be equal to that of a free electron, namely, A^{**} = 120 A / cm^2 K^2 [41,42].

The reverse saturation current can be determined experimentally by extrapolating the linear part of the plot of $\ln J_d$ *versus* V and taking the intercept with the J-axis. As an example, the value of J_s for Al/PTOPT/ITO structure was calculated to be 10^{-15} A / cm^2 [16].

Under illumination, an organic Schottky diode absorbs photons. This absorption process leads to creation of excitons that may later dissociate into

electrons and holes. Thus, the net current under illumination is a combination of the photogenerated current and the thermally emitted current.

As stated above, the dark current is mainly due to the majority carriers whereas the minority carriers have an insignificant contribution. On the other hand, under illumination of, say metal/p-type semiconductor junction, the change in majority carrier (hole) concentration in the valence band will be insignificant while the change in the minority carrier (electron) concentration in the conduction band will be significant. Thus, the observed photocurrent under illumination can be considered as due solely to the generation of the minority carriers.

For p-type polymer/metal Schottky diode, there is an accumulation of electrons in the polymer in the dark near the interface as shown in Fig. 3.4 (a). These electrons will recombine with the excess holes generated by illumination in the depletion region, while the photogenerated electrons drift toward the surface under the influence of the field of the barrier potential. This process finally leads to an equilibrium condition where a new effective Fermi level is established as shown in Fig. 3.4 (b).

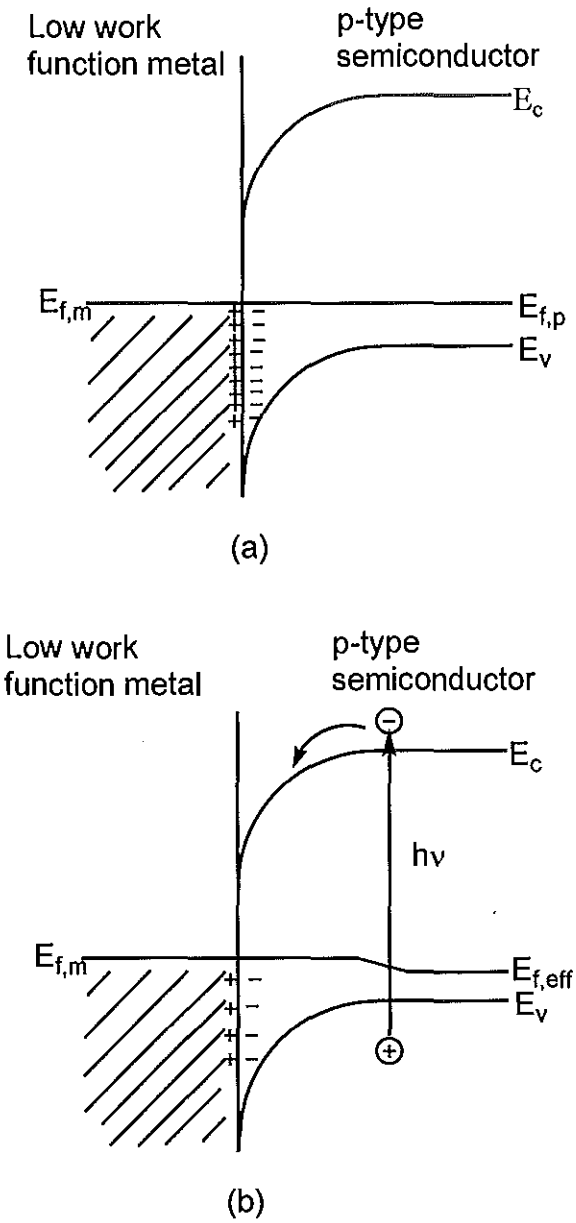

Fig. 3.4 Energy band diagram of metal/p-type semiconductor (a) in the dark, and (b) under illumination.

The I-V characteristics under illumination is given by

$$J = \mathrm{J_{ph}} - \mathrm{J_d} \tag{3.5}$$

where J is the net current density, J_{ph} is the photogenerated current density, J_d is the dark current density. Using equation (3.3) and (3.5) the net current density can be described as

$$J = J_{ph} - \mathrm{J_s}\left[\exp\left(\frac{\mathrm{qV}}{\mathrm{nkT}}\right) - 1\right] \tag{3.6}$$

3.2 Action Spectrum

Light of different wavelengths is absorbed at different depth in the conjugated polymer film. The intensity of light at a distance x in a medium is given by

$$I(x) = \mathrm{I_0}\exp[-\delta(\omega)\,\mathrm{x}] \tag{3.7}$$

where I_0 is the intensity inside the medium at $x = 0$, δ is the absorption coefficient of the medium, and ω is the frequency of the light [43]. The quantum efficiency or spectral response or action spectrum of a device is determined by the photocurrent at various wavelengths relative to the number of photons incident on the surface of the device at that wavelength. The effectiveness of a solar cell to convert incident photons of a given wavelength into photocurrent is measured by the incident monochromatic photon to current conversion efficiency (IPCE), which is defined as the number of electrons generated per number of incident photons. In other words, the quantum efficiency

technique measures the fraction of carriers that contribute to the phtogenerated current and it is given by [44,45]

$$IPCE\% = 1240 \frac{J_{sc}}{\lambda P_{in}} \qquad (3.8)$$

where J_{sc} is the short-circuit photocurrent density ($\mu A / cm^2$), λ is the excitation wavelength (nm), and P_{in} is the incident photon flux (W / m^2).

The quantum efficiency of conducting polymer devices may differ for illumination from front (rectifying) side and back (ohmic) side depending on the width of the active region of the device. The active layer of a true Schottky barrier consists of the depletion width, W, plus the effective diffusion length, L, of the carriers involved in photocurrent generation (see Fig. 3.5).

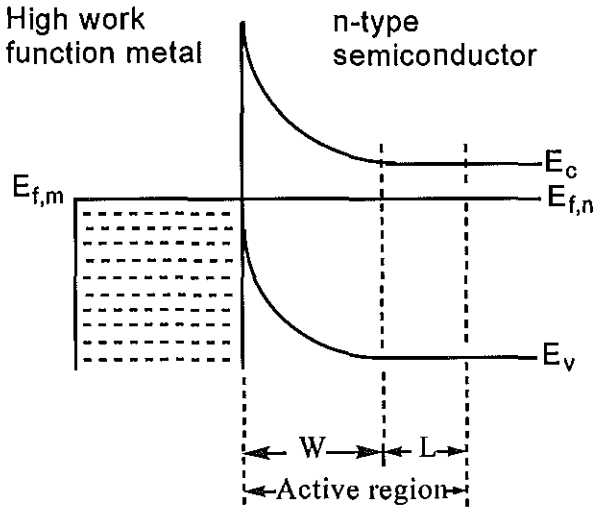

Fig. 3.5 The active region of an n-type semiconductor/metal Schottky barrier.

Any carrier created outside the active region will either recombine or be trapped unless an externally applied field or an electrode field forces it into the metal/polymer interface.

When the thickness of the polymer film is equal to the width of the active region, every photogenerated charge carrier from both sides of the device can reach the interface thereby contributing to the photogenerated current. In such a case, the spectral response matches the absorption spectrum of the polymer independent of the side of illumination. If the polymer film thickness is greater than the average active region width, only the excitons that are able to diffuse into the Schottky barrier region contribute to free carrier generations. In this case the excitons created by illuminating the sample from front (rectifying) side, so long as the electrode is thin, can easily reach the metal/polymer interface and dissociate into free carriers. For this reason, the action spectrum obtained for front side illumination resembles the absorption spectrum of the polymer. However, most of the excitons (electron-hole pairs) generated by back (ohmic) side illumination will either recombine or be trapped during diffusion through the polymer layer towards the Schottky barrier. Therefore for backside illumination the polymer acts as a filter and the action spectrum of the device resembles the inverse of the absorption spectrum of the polymer.

Several researchers working on different semiconductors observed a difference in the action spectra depending on which side of the cell is illuminated [45-54], and this was shown to be in agreement with the proposed theoretical

model by Gosh and Feng [5] for organic solar cells. A comparison of the optical absorption spectrum and the action spectrum of a solar cell can be considered as an alternative means to identify the active junction responsible for the photovoltaic process.

3.3 Fill Factor and Power Conversion Efficiency

The power delivered to a resistive load connected to a photocell under illumination is given by

$$P = \mathrm{IV} \tag{3.9}$$

where I is the net current output of the cell, and V is the voltage drop across the load. Using the value of I from eqn. (3.6) the expression for the power output becomes

$$P = \mathrm{I}_{ph}\mathrm{V} - \mathrm{I}_{\mathrm{s}}\left[\exp\left(\frac{\mathrm{qV}}{\mathrm{nkT}}\right) - 1\right]\mathrm{V} \tag{3.10}$$

The current and voltage, which deliver the maximum power to the load, can be found from eqn. (3.10) by setting the derivative of P with respect to V equal to zero.

$$\frac{dP}{dV} = 0 = \mathrm{I}_{ph} - \mathrm{I}_{\mathrm{s}}\left[\exp\left(\frac{\mathrm{qV}_{\mathrm{m}}}{\mathrm{nkT}}\right) - 1\right] - \mathrm{I}_{\mathrm{s}}V_m\left(\frac{q}{nkT}\right)\exp\left(\frac{qV_m}{nkT}\right) \tag{3.11}$$

where V_m is the voltage at which the maximum power output is delivered. Rearranging eqn. (3.11) one gets

$$[1+\left(\frac{q}{nkT}\right)V_m]\exp\left(\frac{qV_m}{nkT}\right)=1+\frac{I_{ph}}{I_s} \qquad (3.12)$$

The values of V_m and I_m (the value of the current at which $V = V_m$) can be determined by trial and error from the I-V curve of the cell under illumination. Fig. 3.6 shows the maximum power rectangle of a typical solar cell.

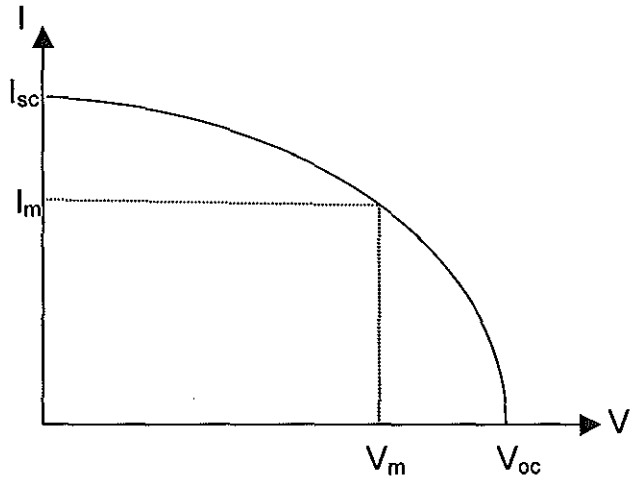

Fig. 3.6 Maximum power rectangle of a typical solar cell. I_{sc} is the short-circuit current of the cell and V_{oc} is its open-circuit voltage.

A fill factor (FF) of a solar cell is a measure of the realizable power from the cell. It is defined as

$$FF = \frac{I_m V_m}{I_{sc} V_{oc}} \tag{3.13}$$

For inorganic solar cells, the fill factor is typically between 0.7 and 0.8 [36]. For undoped organic semiconductors it assumes values less than 0.7 [47-49,55].

The power conversion efficiency of a solar cell is another important parameter that characterizes the cell. It is defined as the ratio of the maximum power from a solar cell of area A to the total power incident on the same device of area A.

$$\eta = \frac{P_{out}}{P_{in}} \tag{3.14}$$

where η is the conversion efficiency, P_{out} the output power, and P_{in} the input power.

In general, the conversion efficiency of a solar cell in percentage is given by [36,56]

$$\eta\% = \left(\frac{I_m V_m}{P_{in}}\right) \times 100\% \tag{3.15}$$

or

$$\eta\% = FF\left(\frac{I_{sc} V_{oc}}{P_{in}}\right) \times 100\% \tag{3.16}$$

3.4 Dependence of Photocurrent on Light Intensity

The short-circuit current of organic and some inorganic solar cells increases with increasing light intensity, P_{in}, and is proportional to P_{in}^{α}, where α is a function of the ratio of the thermally created carrier concentration to the photogenerated carrier concentration. At low intensities α = 1, and at higher intensities α = 0.5. This can be explained using a simple kinetic model. Let $\Delta n = \Delta p$, and p_0 be photogenerated and thermally generated carrier concentrations, respectively. Assuming bimolecular recombination of electrons and holes we have the relationship [57,58]

$$\frac{d(\Delta n)}{dt} = \eta \, I_A - k_r \, \Delta n \, (p_0 + \Delta n) \qquad (3.17)$$

where I_A is the number of absorbed photons per unit volume per unit time, η the primary quantum yield, and k_r a recombination constant. Under steady state conditions, eqn. (3.17) reduces to

$$\frac{d(\Delta n)}{dt} = 0 = \eta \, I_A - k_r \, \Delta n \, (p_0 + \Delta n) \qquad (3.18)$$

Rearranging eqn. (3.18) one gets

$$k_r \, p_0 \, \Delta n + k_r \, (\Delta n)^2 = \eta \, I_A \qquad (3.19)$$

Two limiting cases can be derived from eqn. (3.19):

(a) For $p_0 >> \Delta n$ (low light intensity level), we get

$$\Delta n = \left(\frac{\eta}{k_r p_0} \right) I_A \qquad (3.20)$$

The short-circuit current density, J_{sc}, is proportional to the photogenerated carrier concentration Δn, and the incident light intensity, P_{in}, is proportional to the number of photons per unit volume per unit time, I_A. From this analogy and eqn. (3.20) we get the relationship

$$J_{sc} \propto P_{in} \qquad (3.21)$$

Thus, at low intensity, a linear relationship of short-circuit current with incident light intensity is expected.

(b) For $p_0 << \Delta n$ (higher light intensity level), we get

$$\Delta n = \left(\frac{\eta}{k_r} \right)^{1/2} I_A^{1/2} \qquad (3.22)$$

With the same explanation as in the first limiting case we conclude that

$$J_{sc} \propto P_{in}^{1/2} \tag{3.23}$$

At higher light intensities the number of electrons and holes are almost equal and hence the photocurrent decreases due to an increase in the electron-hole pair recombination.

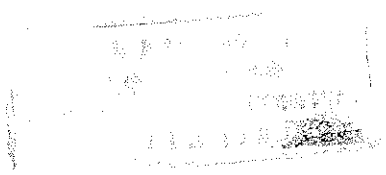

4. Experimental

4.1 I-V Measurement

For electrical characterization, the Al/PTOPT/ITO sandwich structures were prepared as follows. Pre fabricated indium-tin-oxide (ITO)/glass substrate, which is commercially avialable, was cut into pieces of area about 3 cm^2 (Fig. 4.1a). About two-third of these pieces were partly covered with photoresist and the exposed part of the ITO was etched out with a mixture of concentrated hydrochloric acid, nitric acid and water with volume ratio of 48:4:48, respectively. After removing the photoresist with acetone, the ITO-glass substrate was successively cleaned with distilled water, methanol and rinsed with ethanol to get the structure shown in Fig. 4.1b.

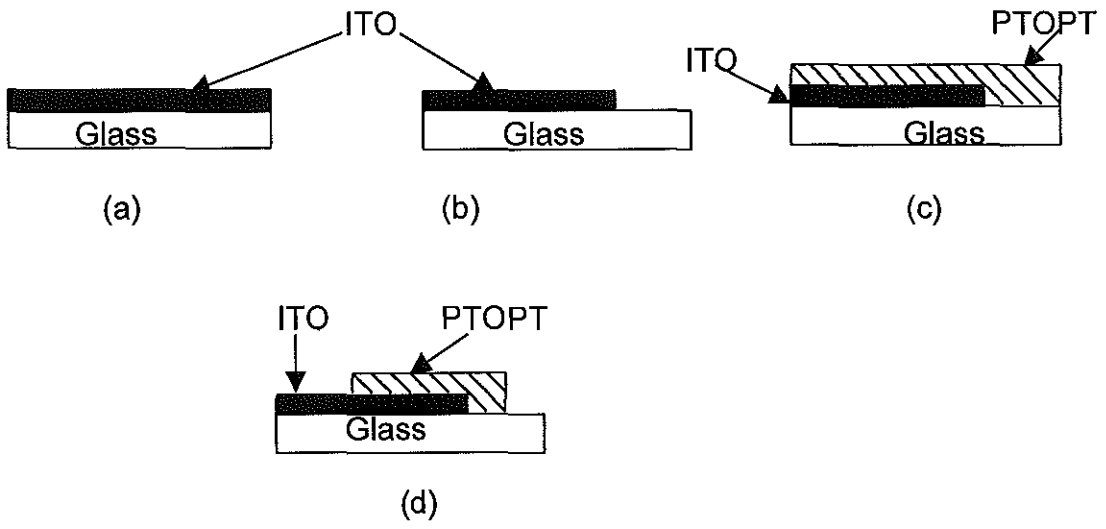

Fig. 4.1 Steps of preparation of the Al/PTOPT/ITO sandwich structure.

Using a programmable spin coater with remote control, PTOPT chloroform solution of concentration 4 mg / ml was spin coated on the ITO-glass substrate at a speed of about 6000-rpm (see Fig. 4.1c). The speed of the spinner is so high that a thin and uniform film is obtained. This was followed by a removal of the PTOPT using chloroform from some parts of the etched as well as the ITO coated glass regions for electrical contacts. The structure thus obtained is shown in Fig. 4.1d. Finally the low work function metal, aluminum, was evaporated on the PTOPT/ITO-glass substrate at a pressure of about 2.5×10^{-6} mbar using Edwards Auto 306 vacuum evaporator. The chemical structure of PTOPT and the Al/PTOPT/ITO sandwich structure are shown in Fig. 4.2.

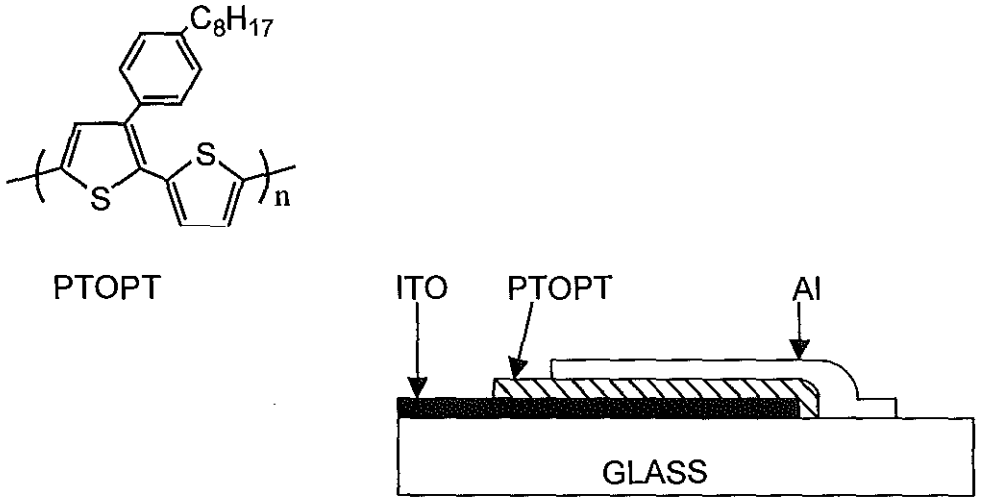

Fig. 4.2 Chemical structure of PTOPT (left) and the schematic diagram of Al/PTOPT/ITO photodiode.

The device formed through all the above processes has an active junction with an area of about 3 mm^2. It will be forward biased when the aluminum electrode is connected to the negative terminal of the voltage source.

The current-voltage characteristics both in the dark and under illumination were measured using HP Pico-Ampere meter (Model 4140B). The meter was interfaced with HP test fixture (Model 16055A) for the dark I-V measurement. The I-V measurement under illumination was carried out by mounting the sample in a sample holder inside a metal box having a 1×1 cm^2 light entrance window. The sample was illuminated with a 150 W tungsten-halogen lamp regulated by an oriel power supply (Model 6329).

4.2 Spectral Response

For spectral response measurement, the incident white light of the halogen lamp passes through an Oriel grating monochromator (Model 7240), which gives a monochromatic light. The monochromator was scanned manually to obtain all possible wavelengths. The schematic diagram of the set-up is shown in Fig. 4.3. The output photocurrent of the photodiode at every wavelength was measured using the HP Pico-Ampere meter. The intensity of the monochromatic light incident on the sample was determined from the spectral response of a calibrated silicon photodiode (Hamamatsu, Model S1336-8BK) by placing it at the sample position. This was done by measuring the photocurrent output of the silicon diode using the Pico-Ampere meter, and normalizing with its spectral sensitivity (measured in Ampere per Watt).

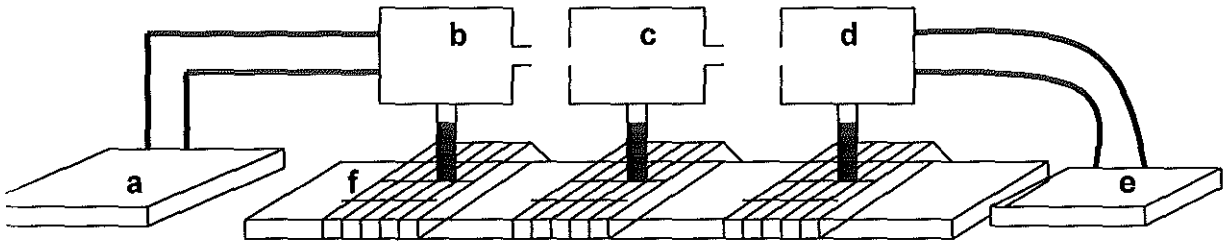

Fig. 4.3 The schematic diagram of the set-up used for the photoelectrical measurements. (a) Power supply, (b) halogen lamp, (c) monochromator, (d) sample holder (e) Pico-Ampere meter, and (f) optical bench.

4.3 Intensity Dependence of I_{sc}

The short circuit photocurrent of the Al/PTOPT/ITO photodiode at various intensities of the incident light was measured by using the Pico-Ampere meter while the intensity of the incident light was measured using a Luxemeter (Model LX-101) by placing its sensor at the sample position. The reading of the Luxmeter was obtained in units of Lux, which was latter changed to watt per centimeter square according to the conversion factor

$$1\text{Lux} = 5 \times 10^{-6}\ \text{W cm}^{-2}.$$

The variation of the light intensity incident on the sample was carried out by controlling the output current of the Oriel power supply. In all the cases no correction was done for reflection from the sample surface.

5. Results and Discussion

5.1 Action Spectrum

The electrical properties of a diode made of PTOPT were studied and it was shown that PTOPT is a p-type semiconductor with very high rectification ratio [16]. Fig. 5.1 shows the photoaction spectra of the Al/PTOPT/ITO sandwich structure. Curves (a) and (b) were obtained under illumination through the ITO and Al electrodes sides, respectively.

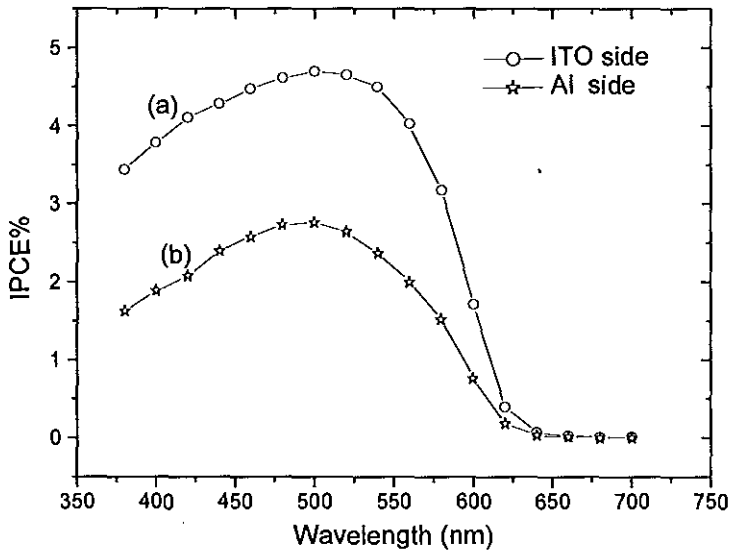

Fig. 5.1 Photoaction spectrum of Al/PTOPT/ITO sandwich structure for illumination through (a) ITO side and (b) Al side.

As can be seen from Fig. 5.1, the two action spectra are similar and the peak is at about 500 nm. The low photocurrent observed for illumination through the Al side is due to the thickness and the poor transmittance as well as high reflectance of

the metal electrode. On the contrary, the ITO electrode is almost transparent for visible light spectrum so that most of the photons incident can pass through the electrode and result in exciton generation in the polymer film.

The photoaction spectra of the Al/PTOPT/ITO photodiode for illumination through (a) ITO side, and (b) Al side, as well as the absorption spectrum of PTOPT are depicted in Fig. 5.2. Normalization was done to the peak value in order to facilitate the comparison between the spectral response and the absorption spectrum.

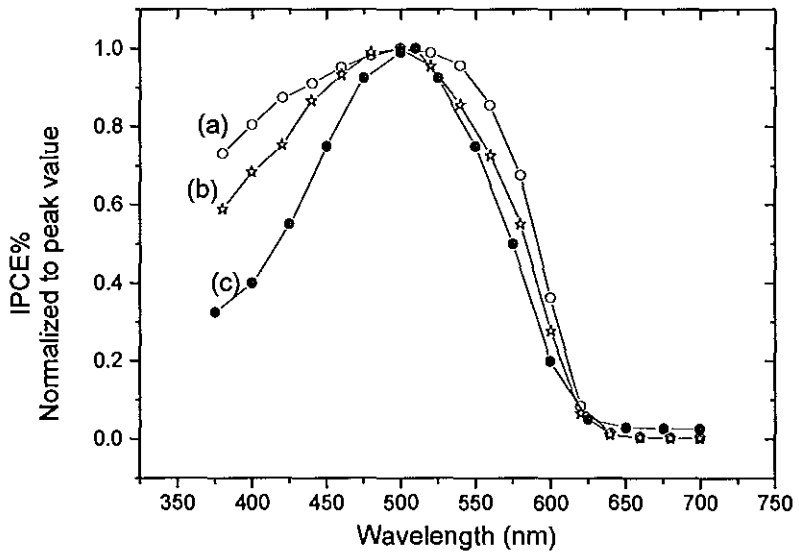

Fig. 5.2 Normalized action spectrum for (a) ITO side illumination, (b) Al side illumination, and (c) normalized optical absorption spectrum of PTOPT coated on pure glass.

As can be seen from Fig. 5.2, the spectral response curves obtained for illumination on both sides match the absorption spectrum of the polymer. This suggests that the thickness of the PTOPT film is less than the width of the active region so that the excitons that were created near the ITO electrode were able to diffuse to the Al/PTOPT junction before they were lost by recombination, or being trapped. The resemblance of the two action spectra with the absorption spectrum of the polymer film may also lead to a conclusion that the active region lies in the polymer and, only the PTOPT layer is responsible for photocarrier generation. This is in agreement with the theoretical model of Gosh and Feng [10] for other organic solar cells. The resemblance of the absorption spectrum with the spectral response irrespective of the direction of illumination was observed in other photovoltaic devices based on organic semiconductors [5,49,52,59].

5.2 Fill Factor and Incident Light Power Conversion Efficiency

The I-V characteristics of the Al/PTOPT/ITO sandwich structure both in the dark and under illumination through the Al side with monochromatic light of intensity 7.4 μWcm^{-2} at 500 nm is shown in Fig. 5.3. No correction was done for the absorption and reflection off the aluminum electrode.

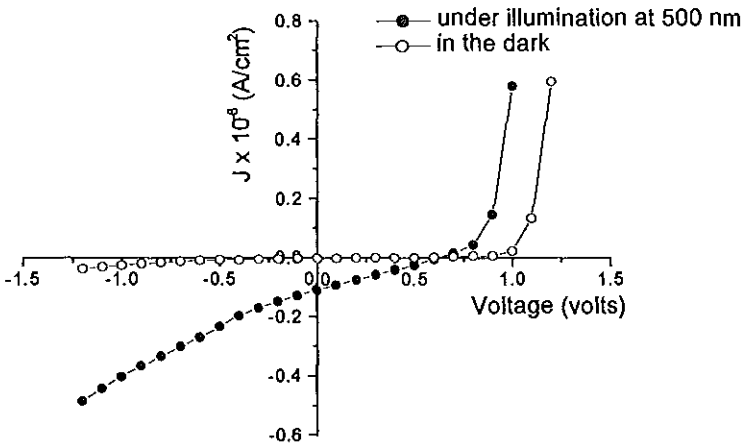

Fig. 5.3 I-V curves in the dark and under illumination through the Al electrode with monochromatic light of intensity 7.4 $\mu W/cm^2$ at 500 nm.

Based on the curve under illumination, the open-circuit voltage (V_{oc}), short-circuit current density (J_{sc}), fill factor (FF), and power conversion efficiency (η in %) were calculated from equations (3.13) and (3.16), and are given in table 1.

Table 1 Photovoltaic parameters of Al/PTOPT/ITO photodiode under illumination of the sample with monochromatic light of intensity 7.4 $\mu W/cm^2$ at 500 nm.

I_{sc} ($\mu A/cm^2$)	V_{oc} (mV)	FF	η %
0.11	630	0.25	0.7

The values of the fill factor and the efficiency are very small when compared with that of the inorganic solar cells. The poor efficiency of this device and any organic solar cell could be explained based on their charge flow mechanisms. The photogenerated electrons and holes in inorganic semiconductors are free whereas absorption creates bound electron-hole pairs (excitons) in organic semiconductors. These excitons can give free carriers by dissociating either at the polymer /metal interface or at some point defect within the bulk of the polymer. The excitons should have high enough lifetimes so that they diffuse into the active interface region before they recombine or being trapped. That means the collection efficiency is highly dependent on the diffusion of the excitons.

The short lifetimes of excitons due to the structural defects of conducting polymers result in low carrier mobilities. The low mobilities of organic semiconductors give small photocurrents, which intern lead to small efficiencies. Thus, the major limitation to the efficiencies of organic semiconductors is their poor mobilities, which are mainly due to the presence of traps.

The poor efficiency of an organic solar cell could be improved by using highly purified materials so that the density of traps could be reduced. The other common way of enhancing the efficiency of organic solar cells is by making blends of two or more materials with different electron affinities. The blends can be either polymer blends or blends created with other molecular acceptors such as Fullerene, C_{60}. One of the materials acts as a donor (D) and the other acts as

an acceptor (A). The free charges created at these D-A hetrojunctions are then transported separately by donor or acceptor material, and are collected at the contact electrodes. Particularly, fullerene, C_{60}, has been widely used as an electron acceptor material with various semiconducting polymers such as poly (3-alkylthiophene) (P3AT) [8], poly(2-methoxy-5-(2′-ethylhexyloxy)-1,4-phenylenevinylene) (MEH-PPV) [8], poly(p-phenylenevinylene) (PPV) [60], and poly(3-(4′-(1″,4″),7″-trioxaoctyl)phenyl)thiophene) (PEOPT) [9] where in all cases higher photoconversion efficiencies than single polymer layer devices were obtained.

Thus, the efficiency of our device could be improved if the polymer PTOPT is blended with an acceptor material(s), and this opens a way to further investigation.

5.2 Dependence of I_{sc} on Incident Light Intensity

. Figure 5.4 shows the behavior of I_{sc} *versus* P_{in} for the Al/PTOPT/ITO device illuminated from the Al side.

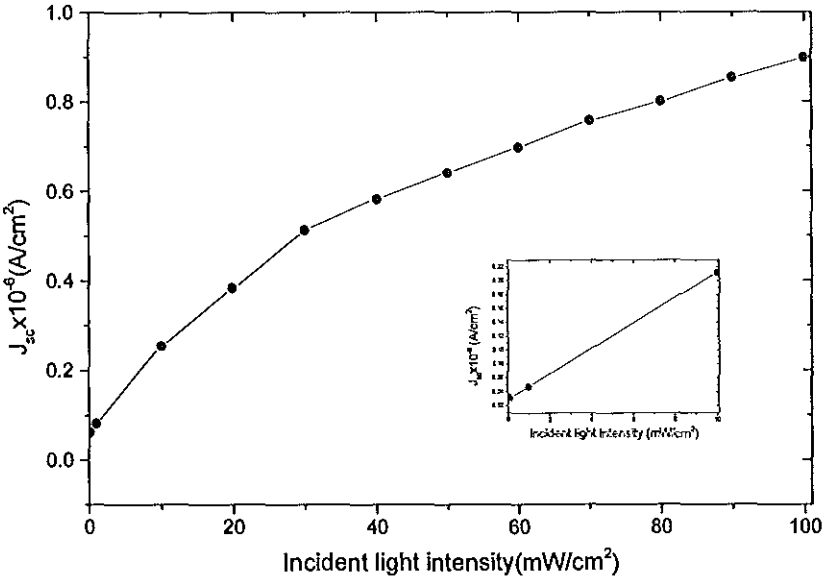

Fig. 5.4 Dependence of photocurrent on incident light intensity. The linear relationship at low light intensities is shown in the inset.

As shown in Fig. 5.4, a linear relationship is observed up to 10 mW/cm^2 as shown in the inset. Figure 5.5 shows the plot of logJ_{sc} *versus* logP_{in} for incident light intensities of 10 mWcm^{-2} and above. The slope of this curve was calculated to be 0.53, which shows that the short circuit current varies non-linearly with the incident light intensity as

$$J_{sc} \propto P_{in}^{0.53}$$

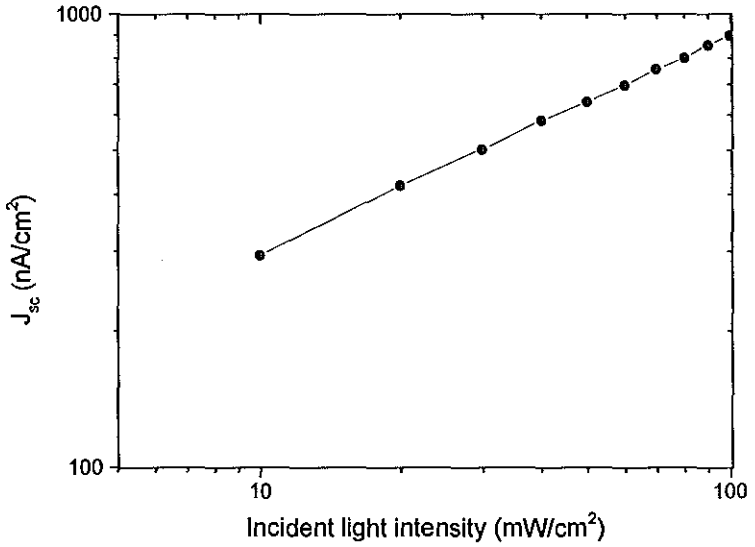

Fig. 5.5 Variation of short-circuit current with incident light intensities.

The linear dependence at low light intensity is due to a low thermal carrier concentration in the cell. The square root dependence of the photocurrent at higher intensities suggests the presence of traps and an increase in the density of recombination centers. The traps could be due to the structural defects in the polymer PTOPT and they enhance charge recombination, which intern shortens the average lifetime of the charge carriers. In other words, the generation of high photocurrent is limited by the intensity dependence of exciton generation, diffusion, recombination, and finally exciton dissociation at the active interface.

Conclusion

In this research work, the photovoltaic properties of Al/PTOPT/ITO sandwich structure have been investigated. The polymer PTOPT shows good spectral response throughout the visible region of the incident light spectrum, giving a peak at 500 nm. The IPCE% at the peak is 2.8 % for illumination through the Al electrode and 4.7 % for illumination through the ITO electrode. The resemblance of the photoaction spectra obtained under illumination from both sides with the absorption spectrum of the polymer has been explained with the model proposed by Gosh and Feng. The short circuit current increases linearly with the incident light intensity up to 10 mW/cm^2, and followed by square root dependence for intensities greater than 10 mW/cm^2. The decrease in the short circuit current at higher light intensities is due to the increase in the recombination rate of electron-hole pairs. From the I-V curve obtained by illuminating the Al/PTOPT/ITO structure from the Al side with monochromatic light (500 nm) of intensity 7.4 mW cm^{-2} a fill factor of 0.25 and incident light power conversion efficiency of 0.7 % were obtained.

References

1. D. Wöhrle, and D. Missner, *Adv. Mater.*, **3** (1991) 129.
2. D.M. Chapin, C.S. Fuller, and G.L. Pearson, *J. Appl. Phys.*, **25** (1954) 676.
3. P. E. Gruenbaum, J.Y. Gan, and R.M. Swanson, *Appl. Phys. Lett.*, **58** (1991) 945.
4. J.M. Li, M. Chong, J.C. Zhu, Y.J. Li, J.D. Xu, P.D. Wang, Z.Q. Shang, Z.K. Yang, R.H. Zhu, and X. Cao, *Appl. Phys. Lett.*, **60** (1992) 2240.
5. A.K. Ghosh and T. Feng, *J. Appl. Phys.*, **49** (1979) 5982.
6. P.J. Reucroft and H. Ullal, *Sol. Energy Mater.*, **2** (1979-1980) 217.
7. B.R. Weinberger, S.C. Gau and Z. Kiss, *Appl. Phys. Lett.*, **38** (1981) 555.
8. N.S.Saricifitci, A.J. Heeger, *in Handbook of Organic Conductive Molecules and Polymers* (Ed: H.S. Nalwa), Wiley, New York, **1** (1997) 437.
9. L.S. Roman, Wendmagen M., L.A.A., Pettersson, M.R. Andersson, and O. Inganäs, *Adv. Mater.*, **10** (1998) 10.
10. R.N. Marks, J.J. M. Halls, D.D.C. Bardley, R.H. Friend, and A.B. Holmes, *J. Phys.: Condens. Matter.*, **6** (1994) 1379.
11. J.J.M. Halls, K. Pichler, , R.H. Friend, S.C. Moratti, A.B. Holmes, *Appl. Phys. Lett.*, **68** (1996) 3120.
12. V.Y. Merritt and H.J. Hovel, *Appl. Phys. Lett.*, **29** (1976) 414.
13. E.R. Menzel and R. O. Loutfy, *Chem. Phys. Lett.*, **72** (1980) 522.
14. D.L. Morel, A.K. Ghosh, T. Feng, E.L. Stogryn, P.E. Purwin, and C. Fishman, *Appl. Phys. Lett.*, **32** (1978) 495.

15. M. Granström, K. Petritsch, A.C. arias, A. Lux, M.R. Andersson, and R.H. Friend, *Nature*, **395** (1998), 257.

16. Bantikassegn W., and O. Inganäs, *Synth. Met.*, **87** (1997) 5.

17. T. Ito, H. shirakawa, and S. Ikeda, *J. Polym. Sci. polym. ED.*, **12** (1974) 11.

18. C.K. Chiang, C.R. Fincher, Y.W. Park, A.J. Heeger, H. Shirakawa, E.J. Louis, S.C. Gau, and A.G. MacDiarmid, *Phys. Rev. Lett.*, **39** (1977) 1098.

19. D. Moses, A. Denensfein, J. Chen, P. McAndres, T. Woerner, A.J. Heeger, A.G. MacDiarmid, and Y.W. Park, *Phys. Rev.*, B **25** (1982) 7652.

20. N. Basescu, Z.-X. Lio, D. Moses, A.J. Heeger, H. Naarmann, and N. Theophilou, *Nature*, **327** (1987) 403.

21. C. Li, Y. Wang, M. Wan and S. Li, *Synth. Met.*, **39** (1990) 91.

22. S. Glenis, G. Tourillon and F. Garnier, *Thin Solid Films*, **139** (1986) 221.

23. G. Horowitz and F. Garnier, *Sol. Energy Mater.*, **13** (1986) 47.

24. P. Panayotatos, D. Parikh, R. Sauers, G. Bird, A. Piechowski and S. Husain, *Solar Cells*, **18** (1986) 71.

25. O. Stenzel, A. Stendal, K. Voigtsberger, and C. Von Boroczyskowski, *Solar Cells*, **37** (1995) 337.

26. G.D. Sharma, S.G. Sangodkar and M.S. Roy, *Thin Solid Films*, **278** (1996) 129.

27. Siegmar Roth, *One Dimensional Metals*, VCH Publishing, INC., New York, NY, 1995.

28. N.F. Mott, and E.A. Davis, *Electronic Processes in Non-Crystalline Materials*, 2nd. ed., Clarendon Press, Oxford, 1979.

29. R. Zallel, *The Physics of Amorphous Solids*, New York, John Willey & Sons, 1983.

30. A.J. Epstein, *in Handbook of Conducting Polymers,* (ed, T. Skotheim), Marcel Dekker, New York, 1986.

31. E. Punkka, M.F. Rubner, J.D. Hettinger, J.S. Brooks and S.T. Hannahs, *Phys. Rev.*, B **43** (1991) 9076.

32. C.O. Yoon, M. Reghu, D. Moses and A.J. Heeger, *Phys. Rev.*, B **49** (1994) 10851.

33. P. Sheng, *Phys. Rev.*, B **21** (1980) 2180.

34. P. Sheng, and J. Klafter, *Phys. Rev.*, B **27** (1983) 2583.

35. E.H. Rhoderick, R.H. Williams, *Metal Semiconductor Contacts,* 2nd. ed., Clarendon, Oxford, 1988.

36. Donald A. Neamen, *Semiconductor Physics and Devices,* Basic Principles, Richard D. IRWIN, INC, 1992.

37. M. Berggren, O. Inganäs, G. Gustafsson, J. Rasmusson, M.R. Andersson, T. Hjertberg and O. Wennertröm, *Nature*, **372** (1994) 444.

38. A. Assadi, M. Willander, C. Svensson, and J. Heldberg, *Synth. Met.*, **53** (1995) 1972.

39. P. Dyreklev, G. Gustafasson, O. Inganäs, and H. Stubb, *Solid State Comm.*, **82** (1992) 317.

40. S.J. Fonash, *Solar Cell Device Physics,* Academic Press, New York, 1981.

41. H. Tomozawa, F. Braun, S. Phillips, A.J. Heeger, and H. Kroemer, *Synth. Met.*, **22** (1987) 63.

42. H. Koezuka, and S. Etoh, *J. Appl. Phys.*, **54** (1983) 2511.

43. Peter W. Milloni, and Joseph H. Eberly, *Lasers,* John Wiley & Sons, New York, 1988.

44. N. Vlachopoulos, P. Liska, J. Augustynski, and M. Grätzel, *J. Am. Chem.Soc.*, **110** (1988) 1216.

45. R.O. Loufty, and J.H. Sharp, *J. Chem. Phys.*, **71** (1979) 1211.

46. S. Glenis, G. Horowitz, G. Tourillon, and F. Garnier, *Thin Solid Films*, **111** (1984) 93.

47. M.S. Roy, G.D. Sharma, and S.G. Sangodkar, *Synth. Met.*, **81** (1996) 15.

48. S. Curran, S. Roth, A.P. Davey, A. Drury, and W. Blau, *Synth. Met.*, **83** (1996) 239.

49. G.D. Sharma, M.S. Roy, S.G. Sangodkar, and S.K. Gupta, *Synth. Met.*, **83** (1996) 1.

50. G.A. Chamberlain, *Solar Cells*, **8** (1983) 47.

51. F.-R. Fan, and L.R. Faulkner, *J. Chem. Phys.*, **69** (1978) 3341.

52. S.-A Chen, and Y. Fang, *Synth. Met.*, **60** (1993) 215.

53. Y. Fang, and S-An Chen, *Synth. Met.*, **52** (1992) 261.

54. G.A. Chamberlain, *J. Appl. Phys.*, **53** (1982) 6262.

55. G.D. Sharma, M.S. Roy, and S.K. Gupta, *Synth. Met.*, **88** (1997) 57.

56. Donald A. Seanor, E*lectrical Properties of Polymers,* Academic Press, 1982.

57. H. Meier, *Organic Semiconductors,* Verlag Chemie, Berlin, 1974.

58. F. Gutmann, and L.E. Lyons, *Organic Semiconductors*, Wiley, New York,1967.

59. G.D. Sharma, *Synth. Met.*, **74** (1995) 227.

60. J.J. Halls, K. Pichler, R.H. Friend, S.C. Moratti, A.B. Holmes, *Synth. Met.*, **77** (1996) 277.